Journal of The Electrochemical Society, **157** (3) H268-H271 (2010)
0013-4651/2010/157(3)/H268/4/$28.00 © The Electrochemical Society

Effect of Threading Dislocations on Local Contacts in Epitaxial ZnO Films

C. Y. Lin,[a,b] W.-R. Liu,[a,c,z] C. S. Chang,[a] C.-H. Hsu,[a,c] W. F. Hsieh,[a,d,z] and F. S.-S. Chien[b,z]

[a]*Department of Photonics and Institute of Electro-Optical Engineering, National Chiao Tung University, Hsinchu 300, Taiwan*
[b]*Department of Physics, Tunghai University, Taichung 407, Taiwan*
[c]*National Synchrotron Radiation Research Center, Hsinchu 300, Taiwan*
[d]*Institute of Electro-Optical Science and Engineering, National Cheng Kung University, Tainan 700, Taiwan*

Local conductance of a ZnO epifilm with a columnar-grain structure was studied by conductive-mode atomic force microscopy. The probe-ZnO junction at the grain boundary with high density edge threading dislocations (TDs) behaves as a Schottky contact while the junction at the epitaxial core behaves as an ohmic contact, resulting in the nonuniformity of conductance throughout the film. The calculated Schottky barrier is 0.4 ± 0.025 eV. The point defects of doubly charged Zn vacancies accumulated at the edge TDs induce local band bending of ZnO, thus contributing to the Schottky nature at the grain boundary.
© 2010 The Electrochemical Society. [DOI: 10.1149/1.3274825] All rights reserved.

Manuscript submitted August 12, 2009; revised manuscript received November 23, 2009. Published January 4, 2010.

ZnO is a promising semiconductor material for various optoelectronic applications such as light emitting diodes, transparent conducting electrodes, and surface acoustic wave devices[1,2] due to its large direct bandgap (3.37 eV) and exciton binding energy (60 meV) at room temperature. Increasing interest in ZnO was enormously boosted in recent years because of the current advances in the growth techniques, which facilitate the fabrication of high quality ZnO epifilms. Heteroepitaxial ZnO films deposited on lattice-mismatched substrates inevitably contain high density threading dislocations (TDs), which entirely propagate throughout the films. Previous studies indicate that the ZnO epifilms grown on *c*-plane sapphire feature a columnar-grain microstructure consisting of an epitaxial core (EC) encompassed by the small-angle boundary region with high density edge TDs.[3] TDs can degrade the electric and optical performance of light emitting devices because of the TD-related leakage current.[4] Moreover, TDs give rise to the defect states in the bandgap, which enhance the deep-level emission (DLE) in the photoluminescence (PL) spectra.[5] These defect states can be partially occupied by negative charges until their energy (E_{dis}) reaches the Fermi energy of ZnO.[6] The negatively charged TDs in semiconductors have been verified by transmission electron microscopy (TEM) [7] and scanning capacitance microscopy.[3,8] Negatively charged TDs can also result in some unusual effects at the metal–ZnO contacts. A reliable and low resistance ohmic-contact metallization is highly expected for device applications.[9] Although several efforts have been devoted to investigate the properties of common metal–ZnO contacts subjected to thermal,[10] plasma,[11] and UV [12] treatments, few studies were focused on the local properties of metal–ZnO contacts. Therefore, it is crucial to study how TDs locally influence the band structure and conductance at the contacts.

In this study, we applied conducting atomic force microscopy (CAFM) to analyze the local contact to the epitaxial ZnO films. The CAFM measurements have been described elsewhere.[13,14] Briefly, a conducting tip scans at a constant contact force over the surface and acts as an electrode to collect the local current through the probe-ZnO junction. The local current–voltage (*I-V*) characteristics reveal that the contact in the EC region behaves as an ohmic contact but that in the boundary region shows a Schottky one. The filling of the dislocation states by negative charges leads to the bending of the conduction band (CB) in the vicinity of the TD lines, thus forming a Schottky barrier. Considering the position of E_{dis}, 0.4 ± 0.025 eV below the ZnO conduction band minimum (CBM), we attribute E_{dis} to the negatively charged Zn vacancies (V_{Zn}^{2-}).

[z] E-mail: liu.wr@nsrrc.org.tw; wfhsieh@mail.nctu.edu.tw; fsschien@thu.edu.tw

Experimental

The ZnO epifilms with a thickness of approximately 1.2 μm were grown on (0001) sapphires by pulsed laser deposition (PLD). The details of the growth conditions and the structure of ZnO epifilms were reported elsewhere.[3,8] The carrier density n_e, mobility, and resistivity are 3.3×10^{17} cm^{-3}, 12 cm^2 V^{-1} s^{-1}, and 1.6 Ω cm, respectively, as obtained by Hall measurement. The X-ray diffraction (XRD) measurements were performed with a four-circle diffractometer at the wiggler beamline BL13A of the National Synchrotron Radiation Research Center, Taiwan, with an incident wavelength of 1.02735 Å. The topographic and current mappings as well as the local *I-V* characteristics were measured by a scanning probe system (Agilent 5500 AFM) with Cr–Pt coated cantilevers. The PL measurements were carried out with a 325 nm He–Cd laser. The light emission spectrum was measured by a Triax-320 spectrometer equipped with a UV-sensitive photomultiplier tube.

Results and Discussion

Structural analysis of XRD and PL.— The ω-rocking curve of the ZnO(0006) reflection was measured, as shown in Fig. 1a. The obtained mosaic spread of the ZnO film is 0.0564°, which strongly supports the good crystalline quality of the ZnO epilayers. The lattice parameters of the ZnO layer are $a = 3.244$ Å and $c = 5.221$ Å, which were determined by fitting the positions of several Bragg reflections. Compared to the bulk values of a ZnO wafer, $a = 3.249$ Å and $c = 5.206$ Å, the ZnO epitaxial films experience a tensile strain (~0.28%) along the normal to the surface and a compressive strain (~0.15%) along the lateral direction. The tilting and twisting angles as well as the coherence lengths along the normal to the surface and lateral direction are 0.052 and 0.19° and 519 and 90 nm, respectively, extracted from the analysis of the Williamson–Hall plot.[3] The TD densities of the edge and screw types calculated from the XRD data are 5.5×10^9 and 7×10^7 cm^{-2}, respectively, which implies that the edge type is dominant in the film. The PL spectrum at room temperature, as shown in Fig. 1b, exhibits a very weak DLE and a narrow near-band edge (NBE) emission at 3.305 eV with a full width at half-maximum (fwhm) of ~80 meV, which is dominated by the free exciton emission. The narrow NBE emission and low DLE are a signature of good optical performance. Therefore, both the XRD and PL results corroborate the high quality of ZnO films.

Common metal–ZnO contact by Pt electrodes.— The *I-V* characteristic of a common Pt–ZnO contact indicates an ohmic contact, as shown in Fig. 2a. The top Pt electrode was deposited by sputtering. The band diagram of Pt and ZnO (Fig. 2b) shows a significant gap between the Fermi energy of Pt (E_F) and the CBM of ZnO,

Downloaded on 2014-04-24 to IP 140.113.38.11 address. Redistribution subject to ECS terms of use (see ecsdl.org/site/terms_use) unless CC License in place (see abstract).

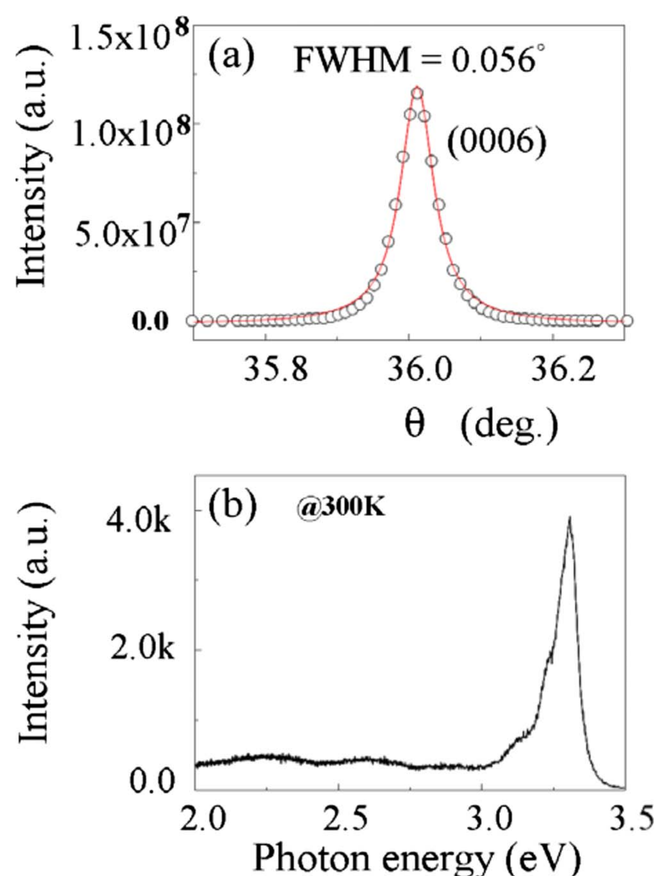

Figure 1. (Color online) (a) ω-rocking curve of the ZnO(0006) reflection and (b) PL spectrum measured at room temperature.

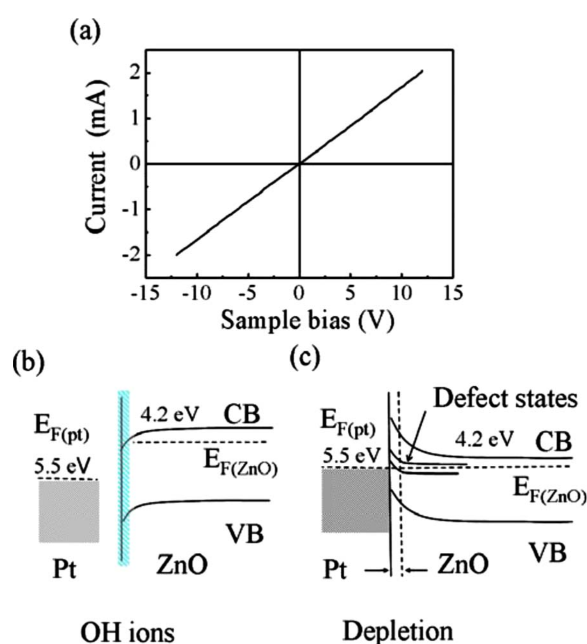

Figure 2. (Color online) (a) *I-V* curve of the normal contact between the Pt electrode and the ZnO epifilm and [(b) and (c)] band diagrams of Pt and ZnO films with the absorption of OH ions at the surface before and after contact, respectively.

suggesting the Schottky nature of the contact. However, several examples of metal–ZnO ohmic contacts, such as Au on commercial undoped ZnO substrates[11] and Ti or Ni on PLD-grown ZnO epifilms,[15] have been reported. The degradation of rectification of the metal–ZnO contacts is attributed to the absorption of OH^- ions on the ZnO surface. It results in the downward band bending of ZnO, producing a conductive accumulation layer at the surface. Therefore, the conducting property of ZnO films can be treated as a bilayer system, i.e., the surface layer and the bulk.[16] The carrier density in the surface layer (n_{se}) could be as high as 5.3×10^{20} cm^{-3} and that in the bulk (n_{be}) is 2.5×10^{16} cm^{-3}.[12] The width of the depletion layer is several nanometers only for the high carrier density of the surface layer, as shown in Fig. 2c. Therefore, tunneling becomes the dominant mechanism of carrier transport, leading to the ohmic behavior of the metal–ZnO contacts.

Local metal–ZnO contacts by metal-coated probes.— Figure 3a is the topographic image of the ZnO surface taken by atomic force microscopy (AFM). Figure 3b and c is current mappings under a forward bias of 0.5 V and a reverse bias of −1.5 V, respectively. The conductance of the film is nonuniform, and there is a strong correlation between the topographic and current images, i.e., the locations of current dips coincide with the grain boundaries under both the forward and reverse biases. Figure 4 shows the cross-sectional profiles along the line (A to B) marked in Fig. 3. Although the dips of the current coincide with that of topography, the width of current dips noticeably differs from that of topographic dips. The fwhm of current dips is ~30 nm. The mean intergrain spacing is about 120 nm, obtained from the Fourier transformation of Fig. 3a, as the lateral coherence length derived from XRD is about 90 nm. The difference between these two lengths yields the 30 nm fwhm of the boundary region. Therefore, it can be concluded that the current dip is due to the edge TDs in the grain boundaries.

The local *I-V* curves taken by a CAFM probe on the EC and grain boundary are shown in Fig. 5. An ohmic contact is observed in the EC region, consistent with the result of the common Pt–ZnO contact. However, the contact at the boundary exhibits a Schottky nature. We fitted the *I-V* curve using the typical expression of thermionic emission[17,18]

$$I = AA^{*}T^{2}\ \exp\left(-\frac{q\phi_{B}}{kT}\right)\left[\exp\left(\frac{qV}{\eta kT}\right)-1\right] \qquad [1]$$

where A denotes the area of the contact, A^* is the effective Richardson constant (~32 A cm^{-2} K^{-2} and $m^* \sim 0.27m_0$), ϕ_B is the Schottky barrier height, k is the Boltzmann constant, T is the absolute temperature (300 K), and η is the ideality factor. We obtained $\phi_B = 0.4 \pm 0.025$ eV and η is ~5, assuming that the contact area is ~1000 nm^2. The high η value elucidates that the transport mechanism is not only thermionic emission but also tunneling. The Schottky behavior is attributed to the TD-related band bending and $\phi_B = \Delta E_{dis}$ ($\Delta E_{dis} = E_{dis} - E_{CBM}$ is the depth of the dislocation states). It implies that the depth of the dislocation states is 0.3–0.4 eV below E_{CBM} of ZnO. Consequently, the CB potential barrier is several tenths of an eV, and the acceptor-like states associated with edge TDs locate near the CBM.

The edge TDs of n-type ZnO were investigated by phase reconstruction of electron waves in TEM.[7] A distinct phase shift of the transmitted electron wave induced by the local potential, generated by the charged dislocation line and associated screening of charges, was recognized; but no phase shift was observed in pure screw TDs. The edge TDs behave as acceptor-like trap states with negative charges in the cylinders of radius d with its axis along the dislocation lines, where d is of several angstroms. Tivarus et al. calculated the local CB bending at the edge TDs line close to a metal–semiconductor interface, as shown in Fig. 6a.[19] The existence of negatively charged edge TDs leads to the carrier depletion in the space charge cylinders around the vicinity of the TD line (shown in Fig. 6b), which accounts for the Schottky nature at the boundary and

Downloaded on 2014-04-24 to IP 140.113.38.11 address. Redistribution subject to ECS terms of use (see ecsdl.org/site/terms_use) unless CC License in place (see abstract).

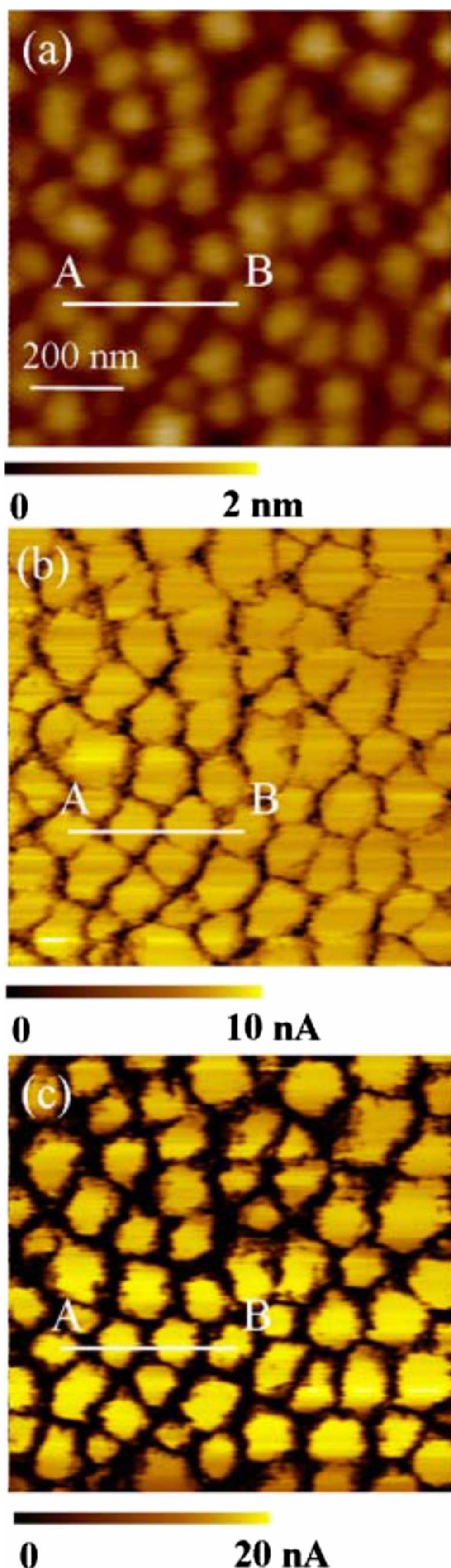

Figure 3. (Color online) (a) AFM topographic image of the ZnO film and the corresponding current mapping images taken under (b) a forward bias of 0.5 V and (c) a reverse bias of −1.5 V.

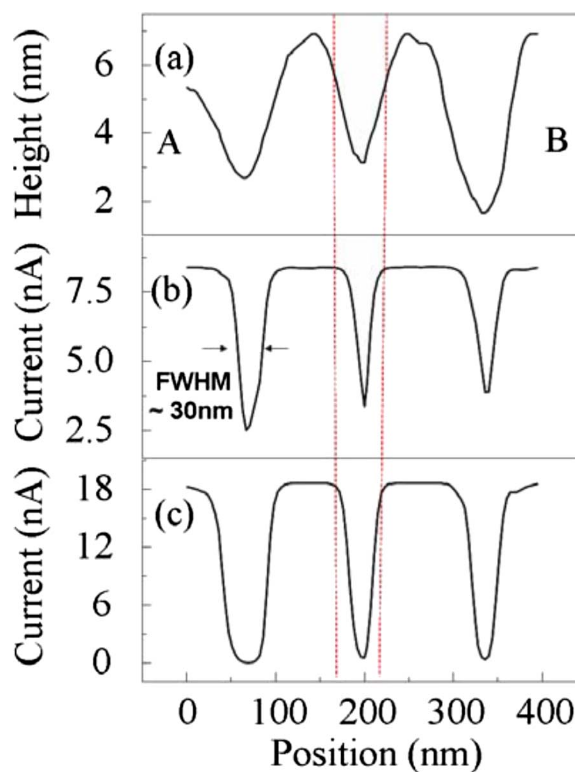

Figure 4. (Color online) (a) Cross-sectional profiles AFM topography and CAFM current under (b) forward bias and (c) reverse bias along the line indicated from A to B in Fig. 3. The dashed lines show the region of the grain boundary.

the conductance mismatch between the EC and boundary region. The radius of the space charge cylinder R can be obtained from the expression[7]

$$R = d\sqrt{\frac{n_{\mathrm{dis}}}{n_{\mathrm{be}}}} \quad [2]$$

Given that n_{be}, the density of trapped charges (n_{dis}),[7] and d are $2.5 \times 10^{16}\ \mathrm{cm}^{-3}$, $5 \times 10^{19}\ \mathrm{cm}^{-3}$, and 0.5 nm, respectively. The calculated diameter (R) of the cylinder is $\sim$22 nm. R is close to the width of the grain boundary obtained from the cross-section profile

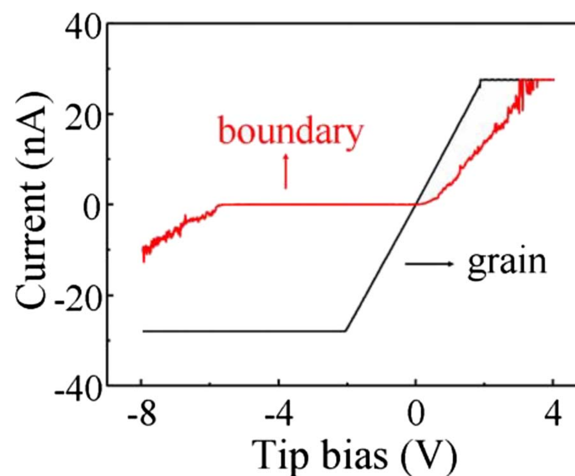

Figure 5. (Color online) Local *I-V* characteristics taken by CAFM on the grain boundary. The current amplifier is saturated beyond ±28 nA.

Downloaded on 2014-04-24 to IP 140.113.38.11 address. Redistribution subject to ECS terms of use (see ecsdl.org/site/terms_use) unless CC License in place (see abstract).

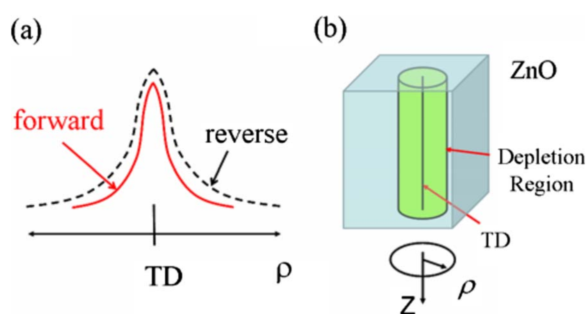

Figure 6. (Color online) (a) Potential diagram of the local conduction band bending near a negatively charged TD line as a function of the distance from the dislocation line under forward and reverse biases and (b) schematic of a charged TD line and the depletion region.

of CAFM. This strongly supports that the dips in current mapping are due to the existence of edge TDs.

From both the CAFM images and current profiles, we observed that the width of the current dips becomes wider when a reverse bias is applied. The reverse bias builds an electric field at the Pt–ZnO interface and causes the decrease in n_{be}. According to Eq. 2, R increases as n_{be} decreases, assuming that n_{dis} is fixed. Effectively, the width of the potential barrier extends with the reverse bias, as illustrated in Fig. 4a.

Assuming that the TDs are electrically inactive and the point defects are accumulated around the dislocation lines caused by the strain field,[20] we suggest that the trapped charges are associated with the point defects. The most abundant native defects in ZnO are the acceptor-like Zn vacancies (V_{Zn}) and the donorlike O vacancies (V_O), according to the calculation using the first-principles pseudopotential method.[21] Here we propose that the defects are doubly charged Zn vacancies (V_{Zn}^{2-}) based on the following facts. First, O vacancies tend to be neutral or positively charged, so V_O is excluded. Second, the Fermi level of the native n-type ZnO is very close to the CBM so that V_{Zn}^{2-} has the lowest formation energy and the estimated energy level of V_{Zn}^{2-} is about 0.4–0.5 eV below E_{CBM},[22] which agrees with our prediction from the *I-V* characteristics. As the density of V_{Zn}^{2-} is sufficiently high, the Fermi level of ZnO is pinned to the defect level of V_{Zn}^{2-}, resulting in the Schottky contact.

ZnO has the same crystal structure as GaN, both belonging to the space group $P6_3mc$. The main defect structures of epitaxial ZnO and GaN films on sapphire substrates are edge TDs. The dislocations are negatively charged in both films.[7,23] However, the electronic behavior of TDs in these films is different. Unlike the Schottky barrier formed at the edge TDs in ZnO films, there is no evidence to show that the edge TDs in GaN significantly affect the current conduction as studied by the probe techniques.[14,23] The charged edge TDs in GaN films should also induce a potential barrier as the theoretical prediction and the analysis of phase reconstruction. The CAFM mapping of GaN may be insensitive to the small variation in potential due to the charged TDs, whereas the probe GaN is a Schottky contact and the defect states are shallow. In contrast to the ohmic Pt–ZnO contact observed in the grain center, one can distinguish the Schottky contact at the edge TD regions from the ohmic background. However, the screw TDs also behave differently in ZnO and GaN films. The screw TDs in GaN introduce leakage paths for the current measured by CAFM, but we did not observe any leakage or other trace of the minor screw TDs in the ZnO film. Further study is therefore necessary to understand the origin of the difference.

Conclusion

The influence of the edge TDs on the electrical properties of the ZnO epifilm grown by PLD on (0001) sapphire was studied by CAFM. The strong correlation between the spatial distribution of TDs and current dip indicates that the edge TDs are negatively charged. The increase in the conduction band in the vicinity of the TDs leads to the Schottky behavior of the Pt–ZnO contact. The bending of the conduction band is caused by the point defects of V_{Zn}^{2-} accumulated along the TD lines, and the defect level of V_{Zn}^{2-} is 0.4 ± 0.025 eV below the conduction band maximum.

Acknowledgments

The authors gratefully acknowledge the support of the National Science Council of Taiwan by NSC contracts 96-2112-M-029-005-MY3 and 97-2112-M-009-013.

Tunghai University assisted in meeting the publication costs of this article.

References

1. A. Tsukazaki, A. Ohtomo, T. Onuma, M. Ohtani, T. Makino, M. Sumiya, K. Ohtani, S. F. Chichibu, S. Fuke, Y. Segawa, et al., *Nature Mater.*, **4**, 42 (2004).
2. X. Y. Du, Y. Q. Fu, S. C. Tan, J. K. Luo, A. J. Flewitt, W. I. Milne, D. S. Lee, N. M. Park, J. Park, Y. J. Choi, et al., *Appl. Phys. Lett.*, **93**, 094105 (2008).
3. W.-R. Liu, W. F. Hsieh, C.-H. Hsu, K. S. Liang, and F. S.-S. Chien, *J. Appl. Crystallogr.*, **40**, 924 (2007).
4. X. A. Cao, J. M. Teetsov, M. P. D. Evelyn, D. W. Merfeld, and C. H. Yan, *Appl. Phys. Lett.*, **85**, 7 (2004).
5. W.-R. Liu, Y.-H. Li, W. F. Hsieh, C.-H. Hsu, W. C. Lee, M. Hong, and J. Kwo, *J. Phys. D: Appl. Phys.*, **41**, 065105 (2008); J. H. You and H. T. Johnson, *J. Appl. Phys.*, **101**, 023516 (2007).
6. H. Alexander and H. Teichler, *Materials Science and Technology*, Vol. 4, Chap. 6, p. 249, North-Holland, Amsterdam (1991).
7. E. Müller, D. Gerthsen, P. Brückner, F. Scholz, Th. Gruber, and A. Waag, *Phys. Rev. B*, **73**, 245316 (2006).
8. W.-R. Liu, W. F. Hsieh, C.-H. Hsu, K. S. Liang, and F. S.-S. Chien, *J. Cryst. Growth*, **297**, 294 (2006).
9. A. A. Iliadis, R. D. Vispute, T. Venkatesan, and K. A. Jones, *Thin Solid Films*, **420–421**, 478 (2002).
10. H. S. Yang, D. P. Norton, S. J. Pearton, and F. Ren, *Appl. Phys. Lett.*, **87**, 212106 (2005).
11. H. L. Mosbacker, Y. M. Strzhemechny, B. D. White, P. E. Smith, D. C. Look, D. C. Reynolds, C. W. Litton, and L. J. Brillson, *Appl. Phys. Lett.*, **87**, 012102 (2005).
12. Y.-J. Lin, C.-L. Tsai, W.-R. Liu, W. F. Hsieh, C.-H. Hsu, H.-Y. Tsao, J.-A. Chu, and H. C. Chang, *J. Appl. Phys.*, **106**, 013701 (2009).
13. P.-J. Gallo, A. J. Kulik, N. A. Burnham, F. Oulevey, and G. Gremaud, *Nanotechnology*, **8**, 10 (1997).
14. J. W. P. Hsu, M. J. Manfra, R. J. Molnar, B. Heying, and J. S. Speck, *Appl. Phys. Lett.*, **81**, 79 (2002).
15. C.-L. Tsai, Y.-J. Lin, Y.-M. Chin, W.-R. Liu, W. F. Hsieh, C.-H. Hsu, and J.-A. Chu, *J. Phys. D: Appl. Phys.*, **42**, 095108 (2009).
16. D. C. Look, H. L. Mosbacker, Y. M. Strzhemechny, and L. J. Brillson, *Superlattices Microstruct.*, **38**, 406 (2005).
17. S. M. Sze, *Physics of Semiconductor Devices*, 2nd ed., Chap. 5, John Wiley & Sons, Englewood Cliffs, NJ (1981).
18. S. H. Kim, H. K. Kim, and T. Y. Seong, *Appl. Phys. Lett.*, **86**, 112101 (2005).
19. C. Tivarus, Y. Ding, and J. P. Pelz, *J. Appl. Phys.*, **92**, 6010 (2002).
20. J. Elsner, R. Jones, P. K. Sitch, V. D. Porezag, M. Elstner, T. Frauenheim, M. I. Heggie, S. Öberg, and P. R. Briddon, *Phys. Rev. Lett.*, **79**, 3672 (1997).
21. A. F. Kohan, G. Ceder, D. Morgan, and C. G. Van de Walle, *Phys. Rev. B*, **61**, 15019 (2000).
22. F. A. Kröger, *The Chemistry of Imperfect Crystals*, 2nd ed., Vol. 2, North-Holland, New York (1984).
23. B. S. Simpkins, E. T. Yu, P. Waltereit, and J. S. Speck, *J. Appl. Phys.*, **94**, 1448 (2003).

Downloaded on 2014-04-24 to IP 140.113.38.11 address. Redistribution subject to ECS terms of use (see ecsdl.org/site/terms_use) unless CC License in place (see abstract).